MULTI-IMAGER STUDY OF TRANSIENTS AND PROPAGATING DISTURBANCES IN ACTIVE REGION LOOPS

D.Berghmans[1], F. Clette[1], E. Robbrecht[2] and D. McKenzie[3]

[1]Royal Observatory of Belgium, Ringlaan 3, B-1180 Brussel, Belgium
[2]Centre for Plasma Astrophysics, K.U.Leuven, Celestijnenlaan 200B, B-3001, Heverlee, Belgium
[3]Montana State University, 264 EPS Building, Bozeman MT 59717, USA

ABSTRACT

On May 13 1998, active region NOAA 8218 was observed in the context of the SOHO/JOP80 campaign by an array of 8 different ground-based and space-born instruments. The emphasis was set on imaging of small-scale and short-lived transient phenomena in this relatively small but rapidly evolving AR. In particular, SOHO/EIT (195 Å), TRACE (171 Å) and YOHKOH/SXT produced subfield image sequences at their respective highest possible rates.

Using an automated recognition scheme, we have been able to collect a wide inventory of transients. By comparing the soft X-ray signature as recorded by SXT with the EUV-signature as collected by EIT and TRACE, we are able to distinguish between various types of active region transient brightenings.

As such we find that the strongest brightenings observed by EIT are indeed the EUV counterparts of the ARTBs seen by SXT. Weaker brightenings seen by EIT do often not have an X-ray counterpart. Moreover, in an extended system of faint quasi-open loops, we find propagating disturbances, with speeds of the order of 100 km/s, both in EIT and TRACE images. These are interpreted as sonic perturbations.

1. INTRODUCTION

From earlier space missions like SMM, Skylab or HRTS it was already known that UV/EUV 'bursts' or impulsive variations occur nearly continuously in active regions. For example, Porter *et al.* (1984) found within an active region, frequent ultraviolet brightenings lasting 40-60 s. Withbroe *et al.* (1985) and Habbal *et al.* (1985) report brightenings in EUV emission lines lasting between 5 and 15 minutes and spatial scales between 5" and 15". With the advent of the Yohkoh spacecraft, a similar intermittency was found in X-rays: (Shimizu *et al.*, 1992, 1997) made an extensive study of active region transient brightenings and made an association with the emergence of tiny magnetic bipoles, suggesting reconnection with preexisting magnetic field.

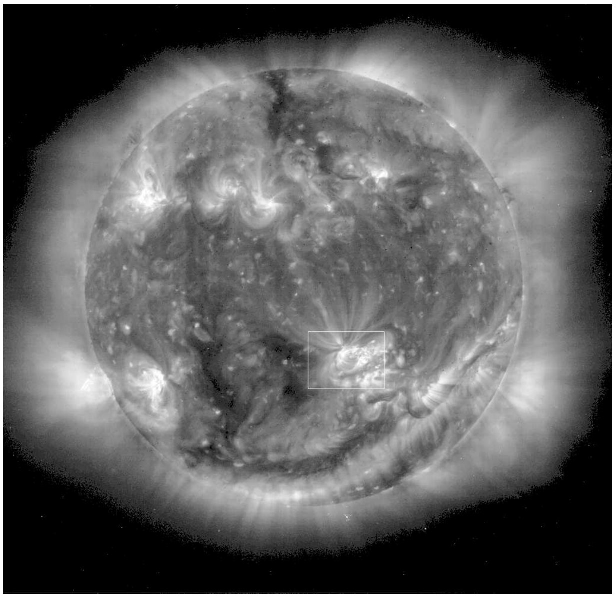

Figure 1. A full disc EIT image in the Fe XII *(195 Å) bandpass, taken at 18h34m UT (5 min after the end of the shutterless mode sequence) showing AR 8218.*

Since the lauch of SOHO, instruments like EIT or CDS observed frequently short-lived explosive brightenings in active regions in the EUV. These were noted in early CDS observations by Mason *et al.* (1997) as strong increases in transition region lines. CDS also observed very rapid time variability in active region loops (Kjeldseth-Moe and Brekke (1998)). The question now arises whether all these observations of brightenings involve truly different phenomena or merely different aspects of the same recurrent process. With this in mind, SOHO JOP 80 was designed as a simultaneous campaign of the best solar instruments operating at their highest cadence on the same target. This approach allows to probe as much aspects as possible from the observed events.

EIT (Delaboudinière *et al.* (1995)) was run in 'shutterless mode' to increase the cadence up to 15 sec. AR 8218 (see Fig. 1) was imaged trough the Fe XII (195 Å) bandpass (peak formation temperature: 1.6 $\times 10^6$ K) from 17h32 up to 18h29. Simultaneously,

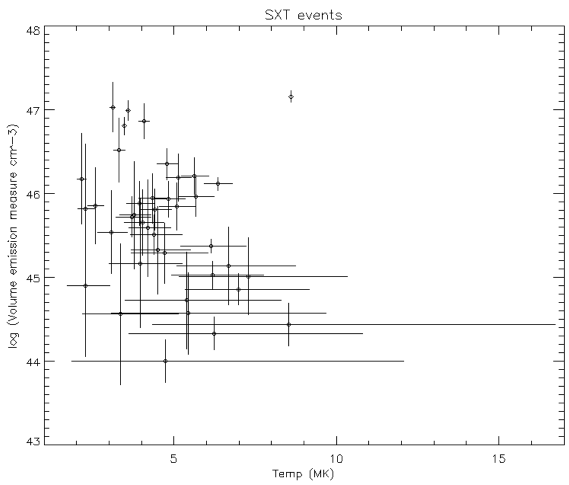

Figure 2. The temperature versus the total emission measure of the brightenings detected by SXT in soft X-rays. The error bars show the 1 sigma uncertainty interval.

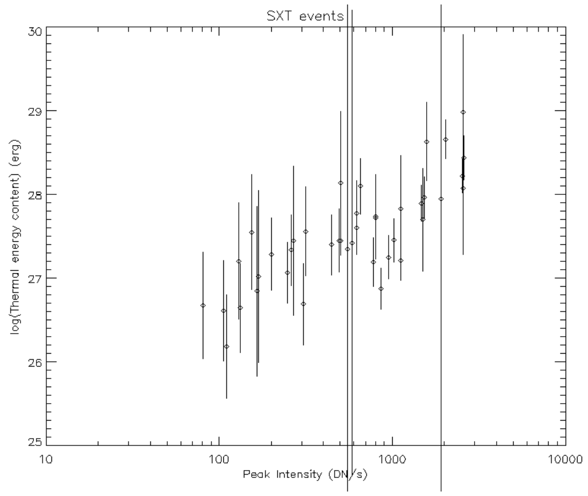

Figure 3. The peak intensity versus the thermal energy content of the brightenings detected by SXT in soft X-rays. The error bars show the 1 sigma uncertainty interval.

TRACE observed in the complementary 171 Å bandpass at a 25 sec cadence. SXT imaged the hotter plasma of the same active region. From 17h21, to 17h57 SXT took images at an 8 sec cadence through the Al/Mg/Mn filter, interleaved at a 98 sec cadence with the Al 1265 Å filter. Several other space born instruments (MDI, CDS, SUMER), as well as two observatories on the ground (in La Palma and Sac Peak) also participated (see Berghmans & Clette (1999) for an overview).

2. DETECTION OF ACTIVE REGION TRANSIENT BRIGHTENINGS

In order to objectively determine the nature of the localised time-variability, we applied an automated scheme (see Berghmans et al. 1998, Berghmans & Clette 1999 for all technical details) that detects localised transient brightenings. In the SXT data sequence, we looked for events with a peak intensity exceeding a calculated background level at the $\Sigma_P = 5\ \sigma_o$ significance level. Neighbouring pixels are assumed to be part of the same event if their light curve exceeds the $\Sigma_E = 3\ \sigma_o$ significance level simultaneously. The duration of the event is traced backwards and forwards in time until the light curves involved go below the $\Sigma_D = 2\ \sigma_o$ significance level. These settings resulted in 41 events brightening in soft X-rays.

Using the Al 1265 Å images that are interleaved in between the high cadence Al/Mg/Mn images, estimations can be calculated for the peak temperature, the total emission measure and the thermal energy of these events. The variety of all these parameters (see Fig. 2 and Fig. 3) covers the same range as those for the ATRBs described by (Shimizu *et al.*, 1992). Therefore we identify the brightenings that our automated detection scheme finds in the SXT data as ARTBs.

Running the automated detection scheme with the same thresholds on the EIT data yields 373 events. We noted that the strongest events in the center of the active region tended to merge with smaller neighbours. We therefore repeated the detection procedure using the higher thresholds ($\Sigma_P = 10\ \sigma_o, \Sigma_E = 6\ \sigma_o, \Sigma_D = 4\ \sigma_o$) which yield a more appropriate estimate of the dimensions of the 68 strongest events. An extensive discussion of the appearance of these events has already been presented by Berghmans & Clette (1999).

In Figure 4, we have superimposed all the detected events on an MDI magnetogram. The active region consists of a leading negative flux region containing two well developped sunspots and a more diffuse trailing positive flux region. Around the two main sunspots a few 'islands' exist of the opposite (i.e. positive) polarity. It can cleary be seen that virtually all SXT events (squares) as well as most of the strongest EIT events (crosses) originate at the neutral line between the main sunspots and these nearby island of opposite polarity. The weaker EIT events (circles) however are spread more randomly over the FOV.

On average, the ARTBs observed with SXT last 5.1 min and become 145 Mm^2 large. In comparison, the 373 brightenings seen with EIT last on average longer (7.8 min) but remain smaller (79 Mm^2, on average).

3. CLASSIFICATION OF THE BRIGHTENINGS IN EVENT CLASSES

A brightening seen in the EIT data on the same place and on the same time as a brightening seen in the SXT data, must obviously be related to each other. In such cases we can define an 'event' of which the brightenings seen by EIT and SXT are the EUV and soft X-ray signatures. Given the limited number of SXT ARTBs, our strategy was to start from the list of brightenings found in the SXT image sequence and look for each of those for corresponding brightenings in the EIT data. After that, we took a look at brightenings seen in the EUV without any (clear) soft X-ray counterpart.

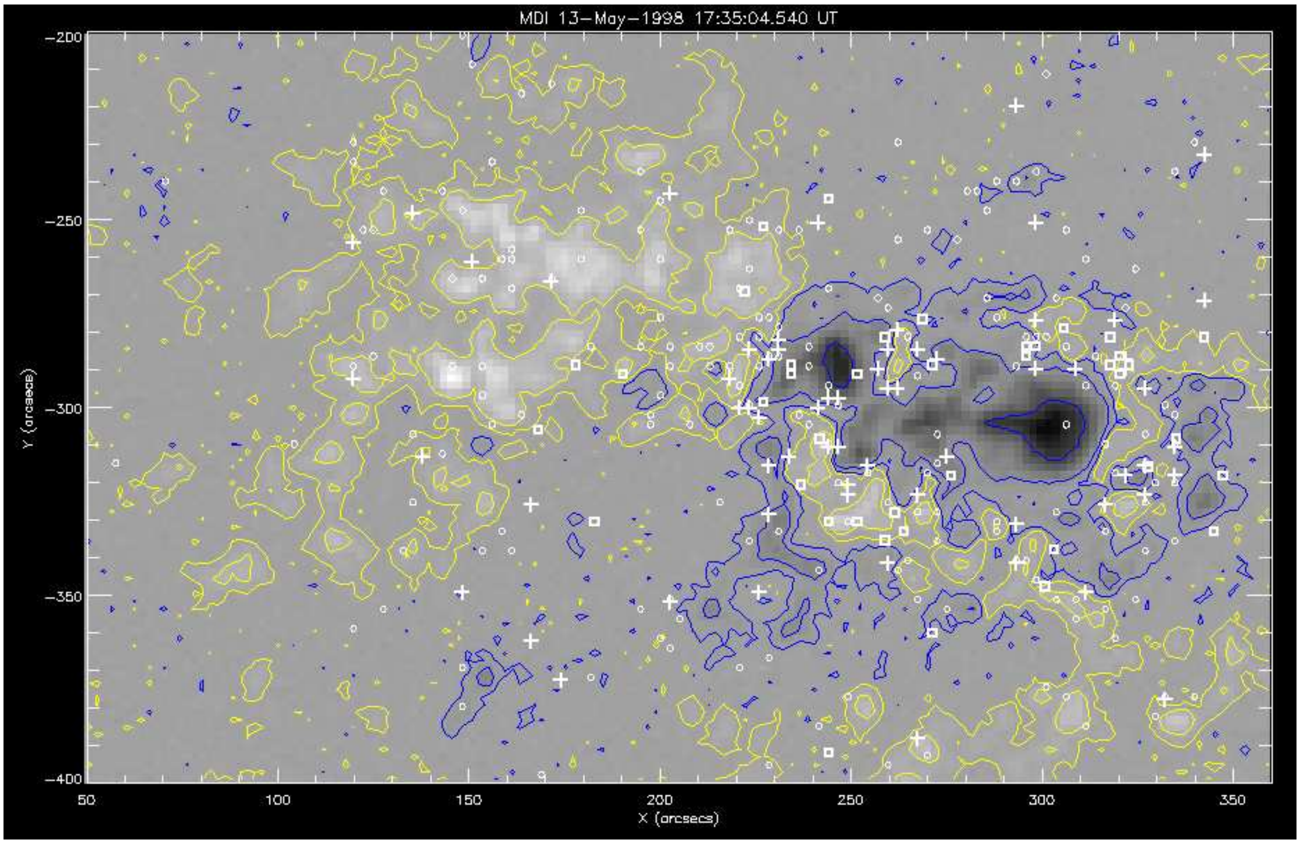

Figure 4. An MDI magnetogram of active region AR8218 with bright contours encircling positive polarity regions (contours at 25, 150 and 900 Gauss) and dark contours encircling negative polarity fluxes (contours at -25, -150 and -900 Gauss). Superimposed we show the location of the events detected in the SXT image sequence (squares) and the events detected in the EIT sequence (high thresholds: crosses, low thresholds: circles).

At first sight, every single SXT event is unique and different from all others. A closer look however reveals that among this variety, one can find recurrent themes which we have baptized 'event classes'. To give the reader an impression of the appearance of the events, we show below a representative example of each event class and discuss the typical characteristics (morphology and evolution) of the members of each class.

3.1. ARTB-type 1, microflare-subflare

The events in this class yield the strongest brightenings in both the EUV and X-rays. Their thermal energy content, as estimated from the SXT data, is above 10^{28} erg and so these events are in the microflare-subflare range. They are all originating near the neutral lines between the main sunspots and the surrounding islands of opposite flux. Often multiple subevents occur recurrently at the same locations. Ussually several EIT brightenings can be attributed to each SXT brightening. Some of these islands of opposite flux look like a cauldron of continuing violent activity both in the EUV and in X-rays. For some other cases the situation is simpler: a brightening X-ray loop preceeded by a smaller brightening EUV-loop with which it shares a common footpoint. An example of such an event is shown in Fig. 5.

3.2. ARTB-type 2, penumbral brightenings

These are smaller events (of the order of 50 Mm^2) with the appearance of small loops which brighten both in X-rays and in the EUV. These little preexisting loops bridge the neutral line just around the main sunspot. Several cases were seen for which the X-ray brightening originated from the two footpoints simultaneously. At the moment of peak intensity the EUV brightening and the soft X-ray brightening seem to fill the same volume. The thermal energy contents peaks for these events in the range 27.3-27.7 erg and the peak X-ray flux is ussualy very small ($<$ 300 DN/sec). An example is shown in Fig. 6.

3.3. ARTB-type 3, long loop brightenings

In contrast to the more impulsive events in the previous categories, these events consist of the gradual brightening of some larger X-ray loops. No signature at all is found in the EUV. These larger loops arch in between the main preceeding and main following polarity. Whereas for the previous events a clear rise and decay phase is seen, the event in this category consists of a rise phase only: the loop stays at it's higher level of emission. The enhancement is more pronounced towards the loop's footpoints but can be found in the whole body of the loop.

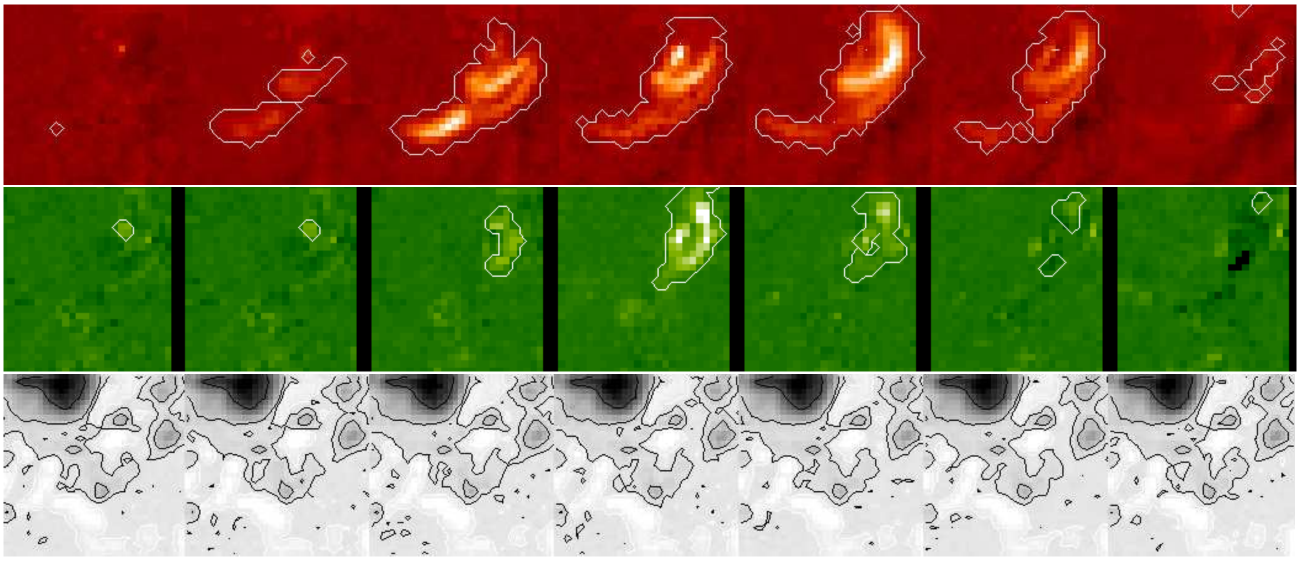

Figure 5. *An example of an ARTB-type 1: a microflare-subflare. Time runs from left (17h30m) to right (17h45). Top row: background subtracted SXT images (contour encircling the detected soft X-ray event); middle row: background subtracted EIT images (contour encircling the detected EUV event), bottom row: MDI magnetograms (contours at ± 25, ± 150, ± 900 Gauss)*

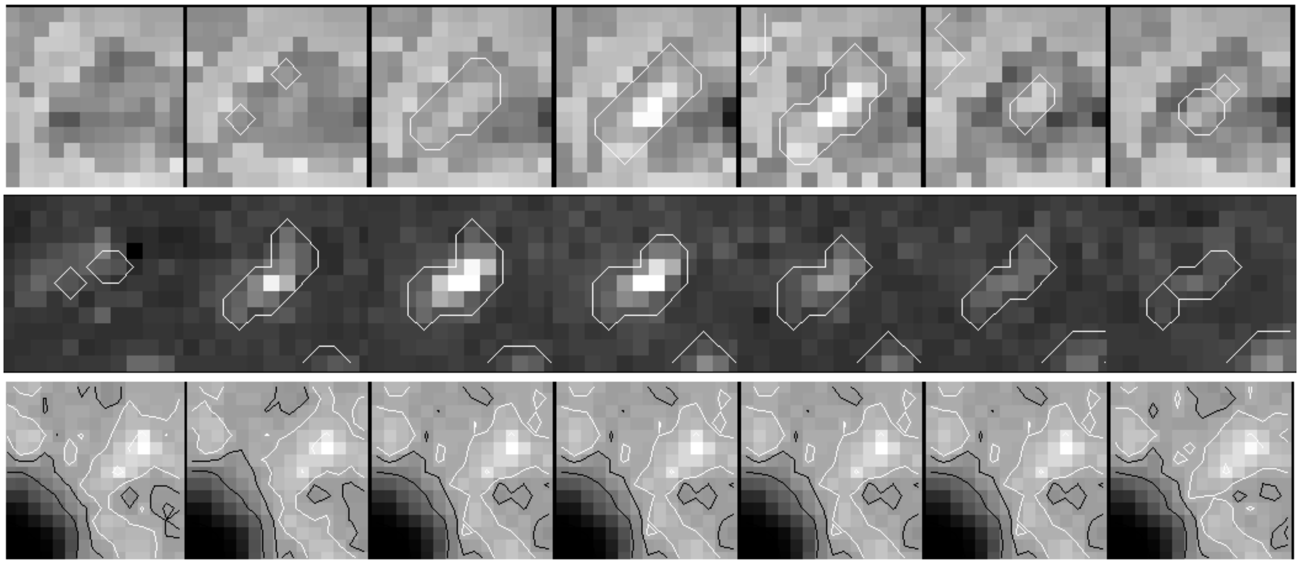

Figure 6. *An example of an ARTB-type 2: a penumbral brightening. Time runs from left (17h33) to right (17h37). Top row: background subtracted SXT images (contour encircling the detected soft X-ray event); middle row: background subtracted EIT images (contour encircling the detected EUV event), bottom row: MDI magnetograms (contours at ± 25, ± 150, ± 900 Gauss).*

3.4. ARTB-type 4, weak EUV brightenings

The events in this class are smaller and weaker EUV brightenings without any X-ray counterpart. They are ussualy detected in the EIT sequence as rather irregularly shaped but the corresponding location in the TRACE images shows clear, brightening loops. This type of brightenings is not restricted spatially to the 'core' of the active region but occurs more uniformily over the field of view.

3.5. ARTB-type 5, footpoint brightenings of extended EUV loops

In the North East of the field of view, a bundle of widely opening fieldlines is present (see Fig. 1). At the footpoints of these fieldlines (see top left of Fig. 4), a last type of events is found. These footpoint brightenings are completely invisible in X-rays and even their EUV signature is weak. These brightenings are the origin of propagating disturbances that travel along the extended EUV loops.

In Fig. 7 we show an example of a somewhat larger example of this event class. The time-evolution of this event is typical: first a moderate intensity enhancement (30%) is observed which is localised to the footpoint of a long field line (17h45m-17h47m UT, pixel P1). This footpoint brightening then expands and propagates along the field lines at a projected speed of the order of 185 km/s. While propagating, the disturbance gets weaker and broader.

We find outward propagating disturbances in virtually all loops within the opening bundle of fieldlines. In Fig. 8 and 9 we show xt-diagrams of propagating disturbances in loops seen in respectively the EIT and TRACE images. From the angle of the diagonal ridges, we can deduce a propagation speed of about 70 to 120 km/s. For the plasma that is visible in the EIT 195 bandpass (peak formation temperature of $1.6 \times 10^6 K$), a sound speed of 192 km/s can be expected. The difference between the observed propagation speeds and the expected sound speed can be bridged by taking into account the projection angle that the flux tubes make with the line of sight. This suggests that the PDS are sonic perturbations. As the PDs travel upward, their absolute amplitude decreases. In the direction along the bright ridges, this decrease is often exponential-like with a decay time of 1.5 to 2 min.

4. DISCUSSION

Based on our ongoing detection and comparison of active region transient brightenings as observed by SXT and EIT, we can already present the following results:

- our detection scheme recovers ARTBs in high cadence SXT data with similar characteristics/dimensions as those described by Shimizu *et al.* (1992, 1997).

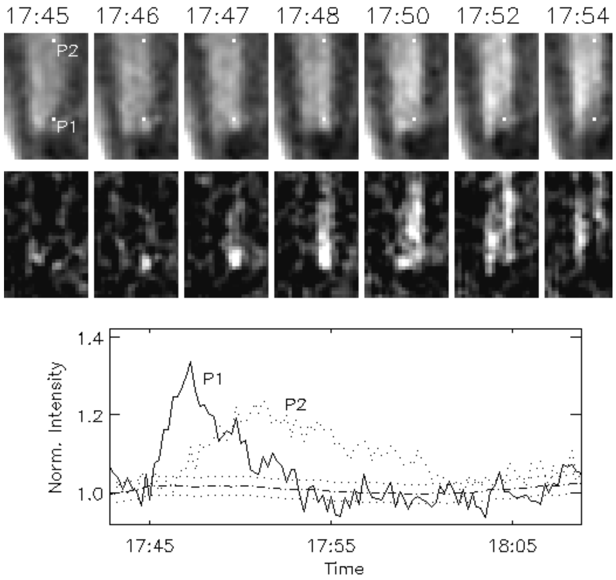

Figure 7. Example of a somewhat larger footpoint brightening event. The top row shows the time-evolution of a footpoint of a long loop as seen in the EIT images. The dimensions of this subfield are 41×75 Mm. The second row shows the same region at the same times but with the background intensity subtracted. Finally the bottom graph shows the time-profile of pixel P1 and P2 in the top row images. The flat dot-dashed and dotted lines represent respectively the background profile and the +/- 1 σ_n interval of pixel P1.

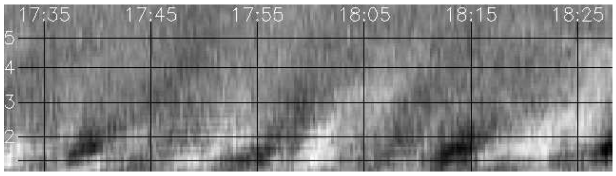

Figure 8. xt-diagram of disturbances propagating along a loop in the EIT images. The vertical axis corresponds to a selected path that outlines one of the loops. Along the horizontal axis we show the time-evolution of the selected loop. Diagonal structures correspond to disturbances propagating along the loop.

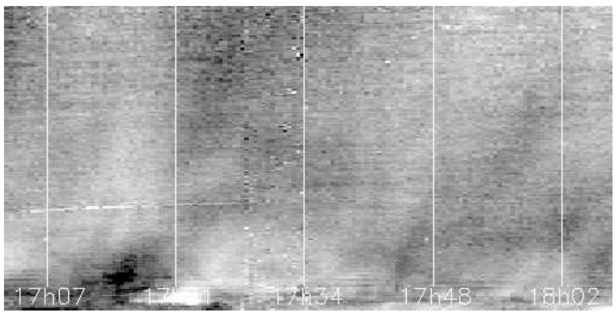

Figure 9. xt-diagram of disturbances propagating along a loop in the TRACE images. As in Fig. 8, the vertical axis corresponds to a selected path that outlines one of the loops. Along the horizontal axis we show the time-evolution of the selected loop.

- In a simulateneous & cospatial high cadence EIT sequence we discover the EUV counterparts of the ARTBs. These are much more numerous by about a factor 5.
- On average, the SXT-ARTB last 5.1 min and become 145 Mm^2 large. In comparison, the EIT-ARTB last longer (7.8 min, on average) but remain smaller (79 Mm^2, on average).
- Based on the SXT data, we estimate the radiative losses of the brightenings range from 10^{25} erg to 10^{29} erg.
- Almost all the SXT-ARTB and the bigger EIT-ARTB originate at the neutral lines between the main sunspot and nearby island of opposite polarity.
- By comparing carefully the EUV signature and the soft X-ray signature it is possible to separate different subpopulations within the group of ARTBs.
- Among the weaker events we find a new subpopulation: small scale brightenings at the footpoints of long loops, followed by wave-like disturbances that propagate upward at an apparent speed of the order of 100 km/s. These propagation speed is compatible with the expected sound speed which suggests that we are seeing sonic perturbations.

The smaller size and the higher birthrate that we find in EIT as compared to SXT, are both consistent with the hypothesis that most of the Fe XII brightenings detected by EIT, correspond to weaker energy releases for which no plasma is heated beyond $2 \times 10^6 K$. These transients are thus undetectable in (higher-temperature) soft X-rays. The brightenings of all 5 different event classes probably originate from small scale, inner-corona reconnection events. We speculate that the different appearance of these classes of events depends on the amount of energy released in such an event, and on the topology of the overlying magnetic field.

ACKNOWLEDGMENTS

The authors would like to thank the whole JOP 80 team for their contribution to this unique data set. This work was supported by the Belgian Federal Services of Scientific, Technical and Cultural Affairs (SSTC/DWTC).

REFERENCES

Berghmans, D. and Clette, F., 1999, Sol. Phys., 186, 207

Berghmans, D., Clette, F. and Moses, D., 1998, Astron. Astrophys., 336, 1039

Clette *et al.*, 1998, http://sohowww.nascom.nasa.gov/~soc/JOPs/jop080.txt

Delaboudinière, J.-P. et al, 1995, Solar Phys., 162, 291

Habbal, S.R., Ronan, R. and Withbroe, G.L. , 1985, Solar Phys., 98, 223

Kjeldseth-Moe, O. and Brekke, P., 1998, Solar Phys., 182, 73

Mason, H.E., Young, P.R., Pike, C.D., Harrison, R.A., Fludra, A., Bromage, B.J.I. and Del Zanna, G. 1997, Solar Phys., 170 ,143

Porter, J.G., Toomre, J., Gebbie, K.B., 1984, Astrophys. J., 283, 879

Shimizu, T., Tsuneta, S., Acton, L.W., Lemen, J.R. and Uchida, Y., 1992, PASJ, 44, L147

Shimizu, T., Tsuneta, S., 1997, Astrophys. J., 486,1045

Withbroe, G.L, Habbal, S.R. and Ronan R., 1985, Solar Phys., 95, 297